A simple method to relate microwave radiances to upper tropospheric humidity

S. A. Buehler and V. O. John

Institute of Environmental Physics, University of Bremen, Bremen, Germany

Received 9 June 2004; revised 24 August 2004; accepted 1 November 2004; published 25 January 2005.

[1] A brightness temperature (BT) transformation method can be applied to microwave data to retrieve Jacobian weighted upper tropospheric relative humidity (UTH) in a broad layer centered roughly between 6 and 8 km altitude. The UTH bias is below 4% RH, and the relative UTH bias below 20%. The UTH standard deviation is between 2 and 6.5% RH in absolute numbers, or between 10 and 27% in relative numbers. The standard deviation is dominated by the regression noise, resulting from vertical structure not accounted for by the simple transformation relation. The UTH standard deviation due to radiometric noise alone has a relative standard deviation of approximately 7% for a radiometric noise level of 1 K. The retrieval performance was shown to be of almost constant quality for all viewing angles and latitudes, except for problems at high latitudes due to surface effects. A validation of AMSU UTH against radiosonde UTH shows reasonable agreement if known systematic differences between AMSU and radiosonde are taken into account. When the method is applied to supersaturation studies, regression noise and radiometric noise could lead to an apparent supersaturation even if there were no supersaturation. For a radiometer noise level of 1 K the drop-off slope of the apparent supersaturation is 0.17% RH^{-1}, for a noise level of 2 K the slope is 0.12% RH^{-1}. The main conclusion from this study is that the BT transformation method is very well suited for microwave data. Its particular strength is in climatological applications where the simplicity and the a priori independence are key advantages.

Citation: Buehler, S. A., and V. O. John (2005), A simple method to relate microwave radiances to upper tropospheric humidity, *J. Geophys. Res.*, *110*, D02110, doi:10.1029/2004JD005111.

1. Introduction

[2] Upper tropospheric humidity plays an important role in the Earth's climate system because it is one of the main factors controlling outgoing longwave radiation [*Held and Soden*, 2000; *Harries*, 1997]. Radiosonde humidity measurements tend to have problems under the dry and cold conditions in the upper troposphere [*Elliot and Gaffen*, 1991]. Furthermore, the radiosonde network is sparse, particularly over the oceans and in the equatorial regions. Thus the only global upper tropospheric humidity measurements come from satellites. Infrared data at 6.7 μm from geostationary and polar orbiting satellites have been used extensively for this purpose. *Soden and Bretherton* [1993] (hereinafter referred to as SB) derived a simple relation between infrared radiances and upper tropospheric humidity:

$$\ln(\mathrm{UTH}) = a + b\,T_b, \tag{1}$$

where UTH is a weighted mean of the fractional relative humidity in the upper troposphere, ln() is the natural logarithm, T_b is the radiance expressed in brightness temperature, and a and b are constants. The original relation by SB contains also a cos(θ) term, where θ is the zenith angle, which was omitted here for simplicity. SB used the radiance Jacobian with respect to relative humidity for the weights in the calculation of UTH.

[3] In the derivation of (1), SB made use of a reference pressure and a dimensionless lapse rate parameter. Various later studies made explicit use of these parameters to improve upon the simple relation. An overview on the different variants of the relation used over the years is given by *Jackson and Bates* [2001]. We will henceforth refer to the method of using (1) to transform radiances (expressed as brightness temperatures) to UTH as the BT transformation method.

[4] The coefficients a and b are typically determined by linear regression, using a training data set of atmospheric temperature and humidity profiles. To get valid coefficients, the data set should capture the atmospheric variability as best as possible. To derive (1), SB assumed that the relative humidity and the temperature lapse rate are constant in the upper troposphere, which is not true for realistic profiles. Vertical structure will thus lead to violations of (1), but the resulting errors will be included in the error analysis, if the error analysis is based on realistic profiles.

[5] The great advantage of the BT transformation method is that radiances and radiance differences can be easily

0148-0227/05/2004JD005111$09.00

transformed to a more intuitive quantity. It is thus very well suited for climatological studies. A disadvantage at first sight is that the UTH defined as the weighted mean relative humidity of the upper troposphere can not be directly compared to other humidity measurements. In particular, the weights in the definition of UTH depend on the atmospheric state, so a drier atmosphere is sampled at lower altitudes. Retrieved UTH spatial fields are thus not defined strictly at a specific level or layer of the atmosphere. While most UTH observations will lie within a roughly 6–8 km layer, this is not guaranteed for all cases.

[6] This difficulty can be overcome by doing the comparison in the proper way, which is to use a radiative transfer model to simulate radiances for all humidity data sets to be compared, and then use the transformation of (1) to map the radiance differences back to UTH differences.

[7] Quite a number of studies have used the BT transformation method to transform infrared radiances into UTH [*Escoffier et al.*, 2001; *Tian et al.*, 2004; *Bates and Jackson*, 2001; *Soden et al.*, 2004], including a recent study on humidity supersaturation with respect to ice as seen by the high-resolution infrared sounder (HIRS) [*Gierens et al.*, 2004]. For microwave sensors, on the other hand, the method has not been much used. While there are many publications about microwave humidity profile retrieval, for example [*Wilheit*, 1990; *Engelen and Stephens*, 1999; *Rosenkranz*, 2001; *Sohn et al.*, 2001], there appear to be only three publications using the BT transformation method.

[8] The first to have used it for microwave data appear to be *Spencer and Braswell* [1997], who applied the method to data from the Special Sensor Microwave humidity sounder (SSM/T-2) in order to study the UTH in the subtropical subsidence zones. They used simulated radiances for radiosonde data from one tropical station to determine the parameters a and b in (1), but neither give the values of a and b, nor a detailed error analysis for the derived UTH, since the focus of the article is on the application rather than on the methodology. *Engelen and Stephens* [1998] published a study comparing HIRS and SSM/T-2 UTH, derived by the BT transformation method. They used a regression on radiances generated for the TOVS Initial Guess Retrieval (TIGR-3) data set [*Chaboureau et al.*, 1998] to determine a and b. Compared to the work by *Spencer and Braswell* [1997], there is a more detailed error analysis, but also no explicit values for a and b. Finally, *Greenwald and Christopher* [2002] used the BT transformation method in their analysis of the effect of cold clouds on UTH derived from the Advanced Microwave Sounding Unit (AMSU) B. Since their main focus is on clouds, there is not much discussion on the BT transformation method, but at least the values $a = 20.95$ and $b = -0.089$ K^{-1} are given for the transformation coefficients.

[9] The goal of the present paper is to demonstrate how the BT transformation method can be applied to AMSU data, to explicitly document the transformation coefficients to use, to discuss the method's performance, and to point out limitations. Although the analysis is carried out for microwave data, some of the new findings can also be applied to the more traditionally used infrared data. To keep things simple we focus only on the clear sky case, although the impact of clouds is an important issue for climatological applications, as shown by *Greenwald and Christopher* [2002], even if the impact of clouds is much less dramatic than in the infrared.

[10] The structure of the paper is as follows: section 2 introduces the microwave data and the retrieval methodology, section 3 presents results and discussion, and section 4 summary and conclusions.

2. Data and Methodology

[11] This section describes the AMSU instrument, the atmospheric data sets used for determining regression coefficients and for validation, the radiative transfer model, and the regression method.

2.1. AMSU Instrument

[12] The Advanced Microwave Sounding Unit (AMSU) B is a cross-track scanning microwave sensor with channels at 89.0, 150.0, 183.31 ± 1.00, 183.31 ± 3.00, and 183.31 ± 7.00 GHz [*Saunders et al.*, 1995]. These channels are called Channel 16 to 20 of the overall AMSU instrument, Channels 1 to 15 belong to AMSU-A. The instrument has a swath width of approximately 2300 km, which is sampled at 90 scan positions. The satellite viewing angle for the innermost scan positions is 0.55° from nadir, for the outermost scan positions it is 48.95° from nadir. This corresponds to incidence angles of 0.62° and 58.5° from nadir, respectively. The footprint size is 20×16 km^2 for the innermost scan positions, but increases to 64×52 km^2 for the outermost positions.

[13] AMSU data for this study was obtained from the Comprehensive Large Array-data Stewardship System (CLASS) of the US National Oceanic and Atmospheric Administration (NOAA). We focus on channel 18 at 183.31 ± 1.00 GHz because its humidity Jacobian peaks in the upper troposphere. Figure 1, which is discussed further in section 2.3, shows this. The method could also be applied to channel 19 at 183.31 ± 3.00 GHz for not too dry atmospheres.

2.2. Atmospheric Data Sets

[14] Two different data sets of atmospheric temperature and humidity altitude profiles were used in this study to determine the transformation parameters a and b: the TOVS Initial Guess Retrieval (TIGR-3) data set and the 60 level sampled ECMWF data set.

[15] The TIGR-3 data set [*Chaboureau et al.*, 1998] consists of approximately 2000 radiosonde profiles from all climate zones and seasons, selected to cover as much as possible the range of atmospheric temperature and humidity variability. The 60 level sampled ECMWF data set [*Chevallier*, 2001] consists of 13495 atmospheric profiles of temperature, water vapor, and ozone. The profiles are sampled in such a way that the atmospheric variability is covered as much as possible, making the data set suitable for regression applications. Some profiles which have water vapor volume mixing ratio values less than 10 ppb were excluded from the calculation.

[16] A third independent data set, consisting of 2 years (2001–2002) of quality controlled radiosonde data [*Leiterer et al.*, 1997] from station Lindenberg, was used for validation. For this data set colocated AMSU measurements were

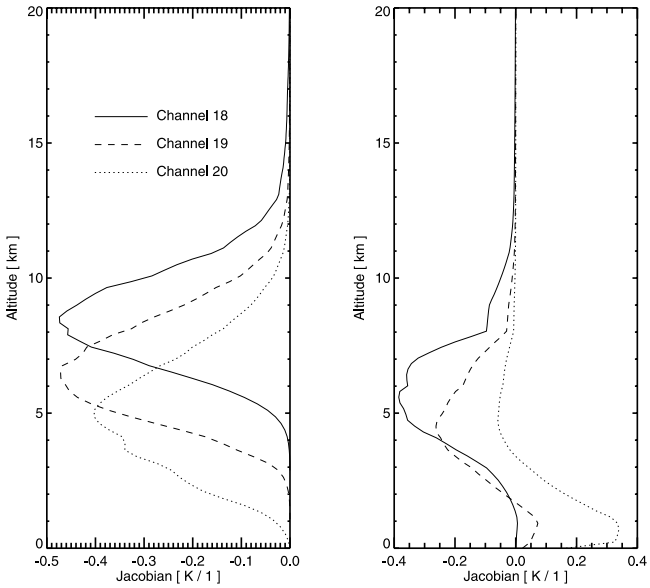

Figure 1. AMSU-B nadir humidity Jacobians for (left) a tropical scenario and (right) a subarctic winter scenario. The scenarios are from *Anderson et al.* [1986]. The Jacobians are in fractional units, so that the values correspond to the change in brightness temperature for a doubling of the mixing ratio at one vertical grid point. Displayed are the Jacobians for channel 18 (solid line), channel 19 (dashed line), and channel 20 (dotted line).

identified with the procedure described in detail by *Buehler et al.* [2004] (hereinafter referred to as BKJ).

2.3. Radiative Transfer Model

[17] The Atmospheric Radiative Transfer Simulator (ARTS), described in detail by *Buehler et al.* [2005], was used to simulate AMSU radiances for given atmospheric states. ARTS is a very general model that can be used from the microwave to the infrared spectral range. Absorption coefficients are obtained by a combination of line-by-line calculation and various continua from the current literature. The model has been validated against a range of other microwave radiative transfer models [*Melsheimer et al.*, 2004] and against a combination of AMSU data and radiosonde profiles, as described in BKJ. The arts-1-0-151 version of the model, which was used for the study, simulates only clear-sky radiances. The program setup was exactly as described in BKJ. The TIGR-3 profiles were interpolated linearly in log pressure onto 100 pressure levels, evenly spaced in log pressure, between the surface and 10 hPa.

[18] The ARTS model was used to simulate radiances for all profiles in the TIGR-3 and ECMWF data sets. Not only nadir radiances were simulated, but also off-nadir radiances corresponding to all AMSU viewing angles. Required geophysical inputs of the model in this case are humidity and temperature profiles, the surface skin temperature, and the surface emissivity. Humidity and temperature profiles were taken from the data sets. The skin temperature was assumed to be equal to the lowest atmospheric temperature. For the TIGR-3 data set the surface emissivity was set to 0.95, for the ECMWF data set it was set to 0.95 for land and to 0.6 for sea. The surface emissivity influences mainly the window channels 16 and 17, but under extremely dry conditions also the sounding channels 18 to 20.

[19] As a rough filter against such extreme conditions, for which relation (1) is not valid, profiles were discarded if the brightness temperature of Channel 20 (T_b^{20}) was not warmer than that of Channel 18 (T_b^{18}). For the simulated clear-sky radiances this occurs only when both channels see the surface, mostly at high latitudes or for high mountains. For all other cases T_b^{20} is warmer than T_b^{18} because its emission comes from lower altitudes in the troposphere. (For real AMSU data the condition $T_b^{20} < T_b^{18}$ can also be used as an indicator of strong convective cirrus clouds, as described by *Burns et al.* [1997].)

[20] The ARTS model was not only used to calculate radiances, but also to calculate the associated Jacobians

$$K_j^{18}(\theta) = \frac{\partial T_b^{18}(\theta)}{\partial x_j}, \tag{2}$$

where j is the vertical grid index, ∂ indicates a partial derivative, and x_j is the water vapor volume mixing ratio (VMR) in fractional units

$$x_j = \frac{\mathrm{VMR}_j^{\mathrm{H_2O}}}{\mathrm{VMR}_j^{\mathrm{Ref}}}. \tag{3}$$

The $\mathrm{VMR}_j^{\mathrm{Ref}}$ are identical to the profile for which the Jacobian is calculated. This type of Jacobian shows the sensitivity of T_b to relative changes in the humidity VMR at each vertical grid point. The profile is assumed to be piecewise linear between the grid points. The grid used is equidistant in the logarithm of the pressure, hence approximately equidistant in altitude. Some example Jacobians for AMSU channels 18 to 20 are shown in Figure 1. Because the Jacobians depend strongly on the atmospheric conditions, Figure 1 shows them separately for a tropical atmosphere and a subarctic winter atmosphere. Channel 18 peaks around 8.5 km for the tropical atmosphere and around 6 km for the subarctic winter atmosphere. Channels 19 and 20 peak at lower altitudes. For the tropical atmosphere they are sounding channels, behaving similarly to Channel 18. However, for the subarctic winter atmosphere the situation is different, Channel 20 is a surface channel, and even Channel 19 has significant influence from the surface.

2.4. Regression Method

[21] We define UTH as

$$\mathrm{UTH}(\theta) = \frac{\sum_j K_j^{18}(\theta)\mathrm{RH}_j}{\sum_j K_j^{18}(\theta)}, \tag{4}$$

where RH_j is the relative humidity at altitude level j. The relative humidity is with respect to liquid water where nothing else is explicitly stated. All altitudes between the surface and 10 hPa are used, although only upper tropospheric altitudes contribute significantly. Note that the UTH defined in this way depends not only on the atmospheric state, but also on the instrument viewing angle, since the

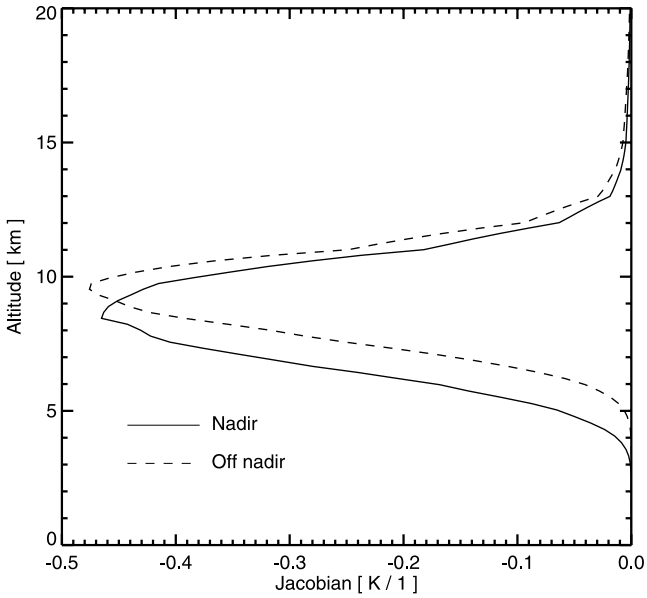

Figure 2. AMSU-B channel 18 midlatitude summer Jacobians for nadir (solid line) and 48.95° viewing angle (dashed line). The latter is the most off-nadir AMSU view. The atmospheric scenario is from *Anderson et al.* [1986].

Jacobian moves to higher altitudes for off-nadir views, as demonstrated by Figure 2. For off-nadir views the instrument simply sees emissions from higher up in the atmosphere.

[22] The UTH values calculated in this way and the simulated radiances were used to determine the parameters a and b of (1) by a simple linear regression. This was done separately for each instrument viewing angle.

[23] Let ΔUTH be the difference between fitted UTH and true UTH:

$$\Delta\mathrm{UTH} = \mathrm{UTH}_{\mathrm{fitted}} - \mathrm{UTH}_{\mathrm{true}}, \tag{5}$$

then we denote the mean value $\overline{\Delta\mathrm{UTH}}$ of ΔUTH as the retrieval bias and the standard deviation $\sigma_{\Delta\mathrm{UTH}}$ of ΔUTH as the retrieval standard deviation. Similarly, we define relative retrieval bias and relative retrieval standard deviation based on the relative difference between fitted and true UTH:

$$\Delta\mathrm{UTH}_{\mathrm{rel}} = \frac{\mathrm{UTH}_{\mathrm{fitted}} - \mathrm{UTH}_{\mathrm{true}}}{\mathrm{UTH}_{\mathrm{true}}}. \tag{6}$$

3. Results and Discussion

[24] This section presents and discusses the regression results and their validation. Furthermore, it explores the potential use of these data for supersaturation studies.

3.1. Regression Results

[25] Figure 3 shows nadir ln(UTH) versus T_b^{18} for the TIGR-3 data set (Figure 3, left) and the ECMWF data set (Figure 3, right). It shows that relation (1) holds very well and that the regression coefficients for the two completely independent data sets are very close. The coefficients for the TIGR-3 data set are $a = 16.50 \pm 0.19$ and $b = -0.0708 \pm 0.0007$ K^{-1}. For the ECMWF data set the coefficients are $a = 16.47 \pm 0.06$ and $b = -0.0702 \pm 0.0002$ K^{-1}. These coefficients are different from the ones reported by *Greenwald and Christopher* [2002], which is probably due to these authors using a different UTH definition. No details are given in the article, but it is likely that they use relative

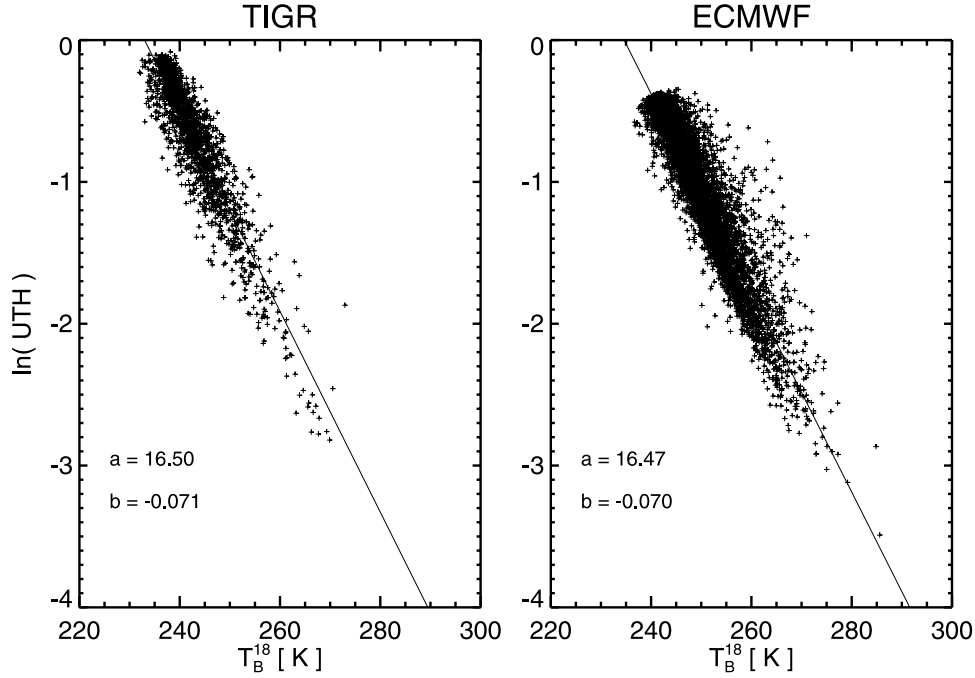

Figure 3. Logarithm of nadir UTH versus nadir T_b^{18} for (left) the TIGR-3 data set and (right) the ECMWF data set.

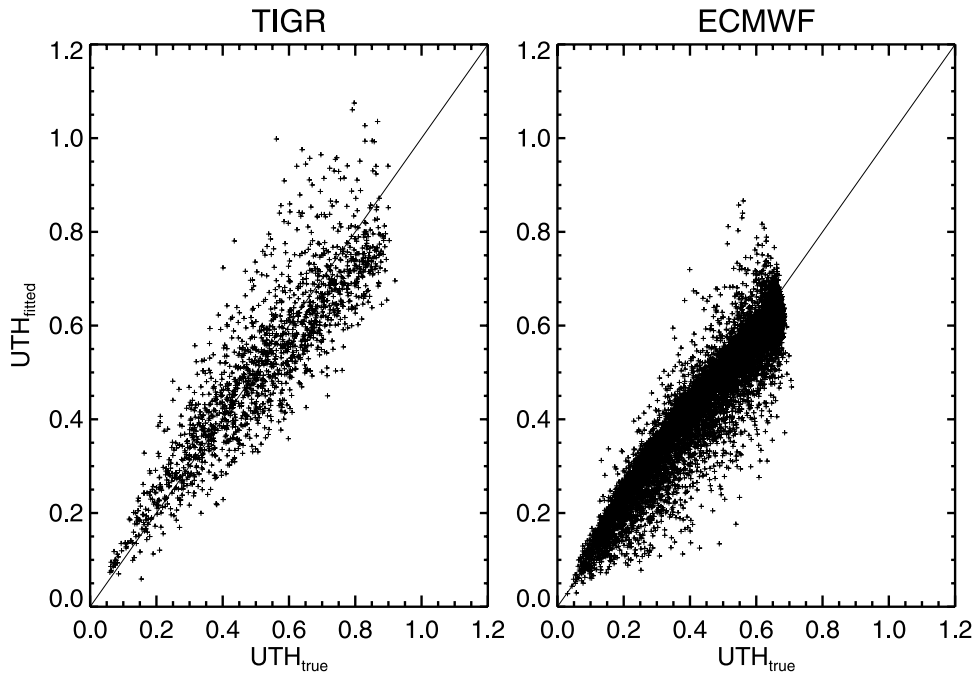

Figure 4. Fitted nadir UTH versus true nadir UTH for (left) the TIGR-3 data set and (right) the ECMWF data set. No artificial noise was added. Only nadir T_b^{18} were used for the regression. UTH is given in fractional units relative to liquid water.

humidity Jacobians, like SB, whereas we use fractional water vapor VMR Jacobians, as described in section 2.3.

[26] The ECMWF parameters have lower errors due to the larger regression data set. To give an impression of the retrieval performance, Figure 4 shows fitted UTH versus true UTH for both data sets. No artificial radiometric noise was added, therefore the figure shows the pure regression noise σ_{UTH}(regr). The source of this noise are variations in the vertical structure of the atmosphere, which lead to small deviations from relation (1).

[27] The overall retrieval bias is very small, −1% RH for the TIGR-3 data set and −0.5% RH for the ECMWF data set. The overall retrieval standard deviation without radiometric noise is 9% RH for the TIGR-3 data set and 5% RH for the ECMWF data set. With added radiometric noise of 1 K standard deviation, a realistic number for Channel 18, the retrieval standard deviation increases to 10% RH and 7% RH, respectively. The bias is not significantly affected by added radiometric noise.

[28] As a safety check, retrieval errors for the ECMWF data set were also calculated for the regression coefficients derived from the TIGR-3 data set. This did not significantly affect the standard deviation, but increased the bias to −5.6% RH. This shows that there is some hidden a priori information in the training data set that can affect the true retrieval bias. We plan to investigate this issue in more detail in a dedicated study, using artificially generated training data sets with known statistics.

[29] Other authors, such as *Soden and Bretherton* [1996] and *Greenwald and Christopher* [2002] have used a normalized reference pressure in relation (1), so that it becomes

$$\ln(p_0\,\mathrm{UTH}) = a + b\,T_b, \tag{7}$$

where p_0 is defined as the pressure of the 240 K isotherm divided by 300 hPa. Quite surprisingly, the introduction of p_0 lead to no improvement for the case with ECMWF data without radiometric noise, but, on the contrary, increased the overall retrieval bias to −10.1% RH and the overall retrieval standard deviation to 9.8% RH. The reason for greater error is that we use the fractional water vapor VMR Jacobian to define UTH, which seems to represent the true sampling altitude better than the relative humidity Jacobian used by other authors. To confirm this, the analysis was repeated for UTH based on relative humidity Jacobians. This increased the overall retrieval bias to −1.4% RH and the overall retrieval standard deviation to 7% RH, without radiometric noise. However, adding the reference pressure in that case decreased the bias to 1% RH and the standard deviation did not change significantly. We conclude that the retrieval of UTH based on the fractional water vapor VMR Jacobian without reference pressure works better than the more traditional retrieval of UTH based on the relative humidity Jacobian with reference pressure.

[30] The ECMWF data set is so large that one can look at the retrieval performance in more detail. For example, Figure 5 displays the bias and the standard deviation (with and without radiometric noise) as a function of $\mathrm{UTH}_{\mathrm{true}}$. Figure 5 (top) shows the absolute quantities, and Figure 5 (bottom) shows the relative quantities. Figure 5 shows that both the bias and the standard deviation depend on the UTH value. Positive bias does not exceed 2% RH for UTH values below 45% RH, and negative bias does not exceed −4% RH for UTH values above 45% RH. Radiometric noise does not affect the bias, only the standard deviation. The standard deviation without radiometric noise σ_{UTH}(regr) increases from 2% RH at a UTH of 5% RH to 5% RH at a UTH of 25% RH, from where on it stays approximately constant.

The effect of radiometric noise scales with the UTH value. One can see this easily from the law of error propagation. Applied to the BT transformation method the law is

$$\sigma_{\Delta\mathrm{UTH}}(\mathrm{radiometric}) = \sqrt{\left(\frac{\partial \mathrm{UTH}}{\partial T_b}\right)^2 \sigma_{T_b}^2} = |b|\mathrm{UTH}\sigma_{T_b}, \quad (8)$$

where σ_{Tb} is the radiometric noise.

[31] It is also interesting to study the retrieval performance as a function of latitude and season. Figure 6 shows bias and standard deviation (with and without radiometric noise) as a function of latitude for JJA and DJF. It has to be noted that these are the statistics for the ECMWF regression data set, which are not necessarily the same as for a true climatology. Zonally averaged Jacobian weighted UTH values for this data set (not shown) have maxima of 40–50% RH in the ITCZ and 50–60% RH at mid latitudes, and minima of 30–40% RH in the subtropics. Bearing this in mind, it can be seen that the retrieval quality displayed in Figure 6 is consistent with Figure 5.

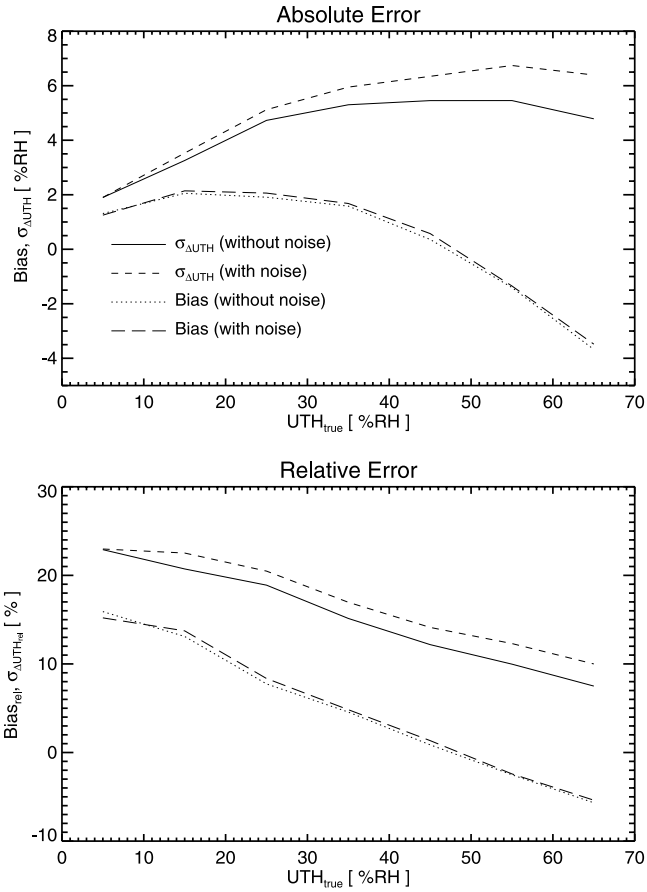

Figure 5. Retrieval performance as a function of true UTH for the ECMWF data set. (top) Absolute quantities and (bottom) relative quantities. Displayed are the retrieval standard deviation with and without radiometric noise (short-dashed and solid lines) as well as the retrieval bias with and without radiometric noise (long-dashed and dotted lines).

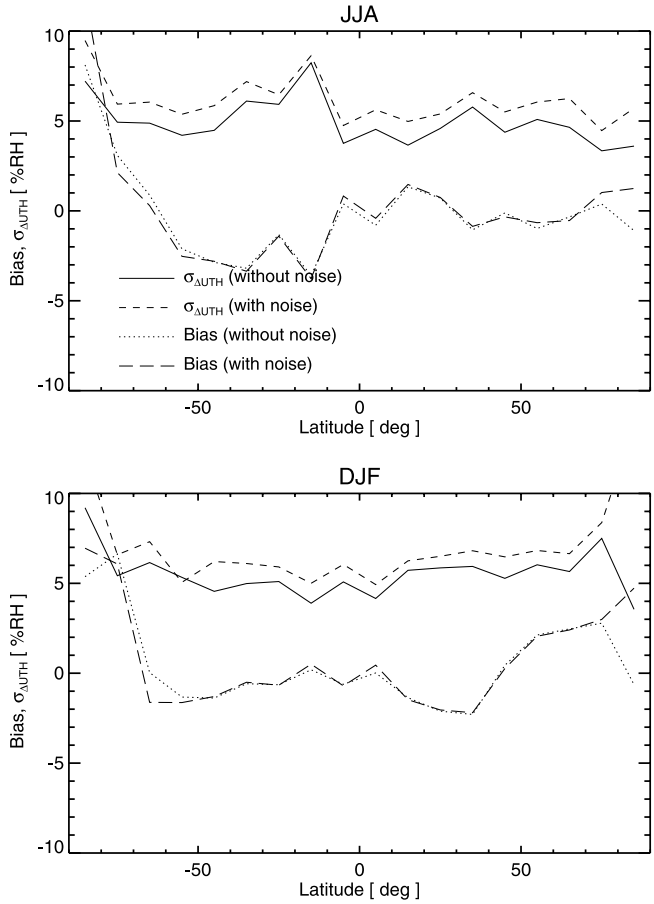

Figure 6. Retrieval performance as a function of latitude for the periods (top) June to August and (bottom) December to February. Displayed are the retrieval standard deviation with and without radiometric noise (short-dashed and solid lines) as well as the retrieval bias with and without radiometric noise (long-dashed and dotted lines). Latitude bins of 10° were used for this analysis.

[32] Overall, there is very little latitudinal and seasonal dependence, except for a significant bias increase in the polar regions, particularly near the south pole in the southern winter. This can be explained by surface effects due to the extremely dry atmospheric conditions, which apparently are not completely removed by the $T_b^{18} < T_b^{20}$ filter. Furthermore, it should be noted that polar conditions are not well represented in the regression data set, because there are only less than 100 polar profiles after applying the filter described in section 2.3.

[33] Judged by Figure 6, there is no need to include latitude-dependent parameters in relation (1). One may wonder whether this conclusion also holds for the relative performance, particularly in the subtropical dry zones. Figure 7 addresses this question. It shows the same results as Figure 6, but for the relative performance parameters, and confirms that the relative retrieval standard deviation increases only slightly in the subtropics.

[34] The discussion so far was only about nadir UTH and nadir T_b^{18}. For off-nadir viewing angles the regression result changes. The solid line in Figure 8 shows the dependence of

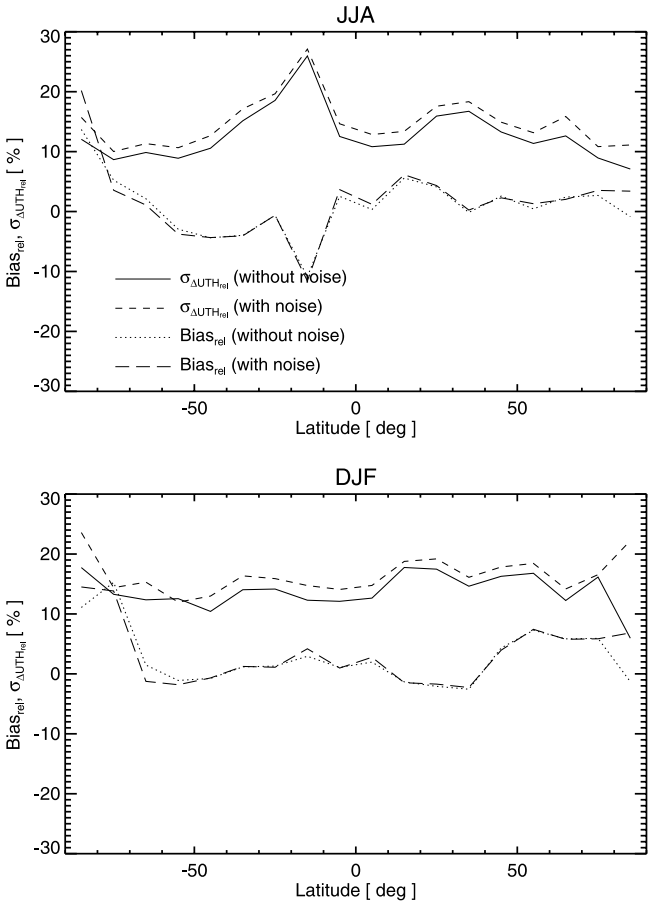

Figure 7. Relative retrieval performance as a function of latitude for the periods (top) June to August and (bottom) December to February. Displayed are the relative retrieval standard deviation with and without radiometric noise (short-dashed and solid lines) as well as the relative retrieval bias with and without radiometric noise (long-dashed and dotted lines).

the offset coefficient a on the viewing angle θ. The original form of (1) in SB is

$$\ln\left(\frac{\mathrm{UTH}}{\cos(\theta)}\right) = a + b\,T_b \tag{9}$$

or

$$\ln(\mathrm{UTH}) = a + \ln(\cos(\theta)) + bT_b, \tag{10}$$

which would mean that a would have the angular dependence

$$a(\theta) = a_0 + \ln(\cos(\theta)). \tag{11}$$

This curve is also indicated as a dotted line in Figure 8. Interestingly, the angular dependence of (11) is opposite from the one obtained from the regression. The solution to this puzzle is that SB did not use an angle-dependent UTH. If we repeat the regression for $\ln(\mathrm{UTH}(\theta = 0))$ versus T_b^{18} we obtain an angular dependence closer to the one derived by SB, which is displayed as a dashed line in Figure 8.

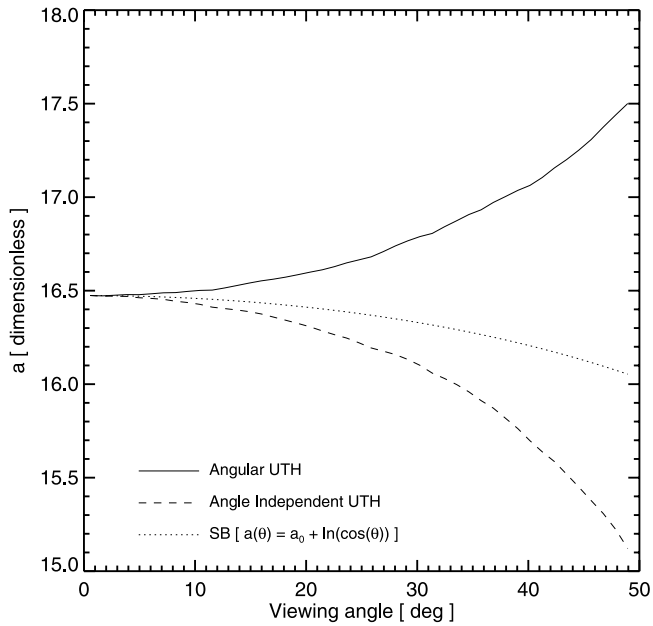

Figure 8. The offset parameter a of (1) as a function of viewing angle for the ECMWF data set. The solid line is the regression result for an angle-dependent UTH, the dashed line is the regression result for an angle-independent UTH, and the dotted line is the theoretical angular dependence derived by SB.

[35] Figure 9 shows the result of a similar analysis for the slope parameter b. The b for an angle-dependent UTH also behaves opposite to the b for an angle-independent UTH. According to the original SB relation b should not have an angular dependence at all, as can be seen from (10).

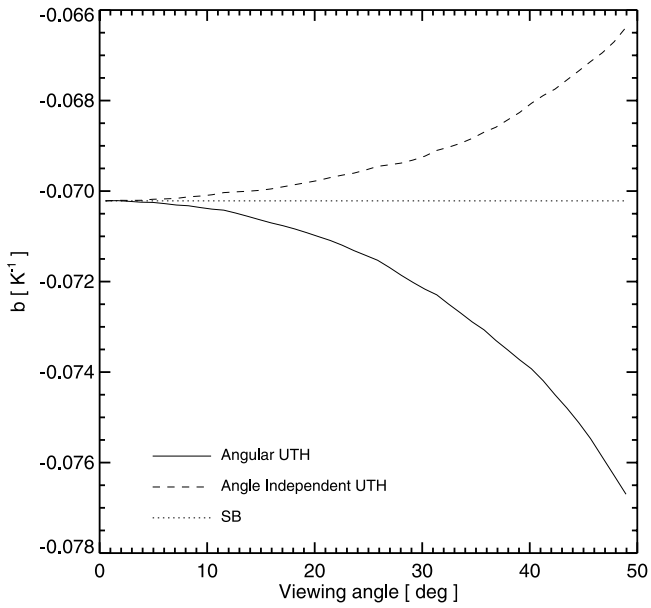

Figure 9. The slope parameter b of (1) as a function of viewing angle for the ECMWF data set. The solid line is the regression result for an angle-dependent UTH, the dashed line is the regression result for an angle-independent UTH, and the horizontal dotted line is the theoretical angular dependence derived by SB.

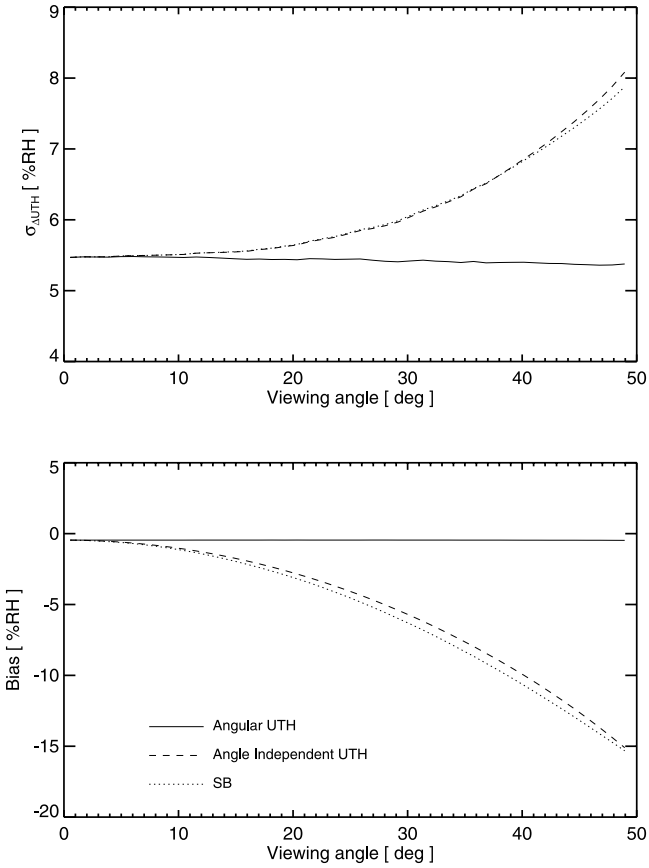

Figure 10. UTH retrieval performance for the ECMWF data set as a function of viewing angle. No artificial radiometric noise was added, so this is the pure regression noise. (top) Retrieval error and (bottom) retrieval bias. The cases shown are using the regression result for angle-dependent UTH (solid line), using the regression result for angle-independent UTH (dashed line), and using the default angular dependence from SB for an angle-independent UTH (dotted line).

[36] From a user point of view it is preferable to have an angle independent UTH, since this depends only on the atmospheric state and not on the instrument. However, since the instrument is sampling higher altitudes for off-nadir views, angle-independent UTH will have higher errors for these views, because the Jacobian used in the UTH definition does not match the actual Jacobian for the off-nadir view. Figure 10 shows that indeed the bias and standard deviation for angle-independent UTH increase with increasing nadir viewing angle, whereas the bias and standard deviation for angle-dependent UTH are approximately constant. Explicit values for the transformation parameters a and b for the ECMWF data set are given in Table 1. It contains the parameters for UTH with respect to liquid water and ice.

3.2. Validation

[37] Colocations of radiosondes and AMSU measurements can be used to validate the retrieved UTH. We used 2 years (2001–2002) of colocations for the radiosonde station Lindenberg and the NOAA 15 and NOAA 16 satellites for this purpose. They are described in detail by BKJ. Colocations where the measured T_b^{18} was not colder than T_b^{20} were discarded in order to screen out cases with significant surface contribution, as described in section 2.3. Furthermore, cases with $T_b^{20} < 260$ K were discarded as a rough filter against clouds, as described in BKJ. No other filters were applied. Figure 11 shows a scatterplot of retrieved $\mathrm{UTH_{AMSU}}$ versus in situ $\mathrm{UTH_{sonde}}$. The $\mathrm{UTH_{sonde}}$ was derived by calculating an AMSU Jacobian weighted mean of the relative humidity according to (4). The standard deviation of the difference between the two is 7% RH, the standard deviation of the relative difference is 18%. These values are in good agreement with the absolute and relative standard deviation from the ECMWF regression with added radiometric noise, which are 7% RH and 16%, respectively, for a radiometric noise level of 1 K.

[38] The standard deviations for the validation are expected to be somewhat higher than the ones from the regression, due to the additional noise inevitable in such a

Table 1. Transformation Parameters Derived From the ECMWF Data Set for Each AMSU Viewing Angle for UTH With Respect to Liquid Water (a_w, b_w) and Ice (a_i, b_i)[a]

θ	a_w	b_w	a_i	b_i
0.55	16.474	−0.0702169	18.341	−0.0764737
1.65	16.472	−0.0702106	18.339	−0.0764688
2.75	16.476	−0.0702271	18.342	−0.0764834
3.85	16.479	−0.0702456	18.345	−0.0764992
4.95	16.479	−0.0702506	18.344	−0.0765034
6.05	16.483	−0.0702774	18.348	−0.0765274
7.15	16.488	−0.0703084	18.353	−0.0765550
8.25	16.490	−0.0703243	18.354	−0.0765713
9.35	16.496	−0.0703634	18.359	−0.0766039
10.45	16.501	−0.0703988	18.363	−0.0766340
11.55	16.503	−0.0704219	18.362	−0.0766454
12.65	16.514	−0.0704853	18.371	−0.0766984
13.75	16.527	−0.0705569	18.381	−0.0767557
14.85	16.540	−0.0706315	18.391	−0.0768198
15.95	16.552	−0.0707031	18.401	−0.0768812
17.05	16.561	−0.0707656	18.407	−0.0769315
18.15	16.572	−0.0708374	18.416	−0.0769950
19.25	16.585	−0.0709191	18.426	−0.0770628
20.35	16.599	−0.0710062	18.436	−0.0771351
21.45	16.612	−0.0710919	18.448	−0.0772143
22.55	16.628	−0.0711956	18.462	−0.0773052
23.65	16.649	−0.0713153	18.478	−0.0774066
24.75	16.665	−0.0714210	18.490	−0.0774960
25.85	16.681	−0.0715289	18.503	−0.0775902
26.95	16.709	−0.0716877	18.525	−0.0777226
28.05	16.740	−0.0718609	18.552	−0.0778808
29.15	16.766	−0.0720197	18.575	−0.0780199
30.25	16.789	−0.0721669	18.592	−0.0781414
31.35	16.806	−0.0722922	18.605	−0.0782481
32.45	16.842	−0.0724969	18.637	−0.0784375
33.55	16.874	−0.0726909	18.664	−0.0786102
34.65	16.907	−0.0728922	18.695	−0.0787986
35.75	16.932	−0.0730668	18.715	−0.0789501
36.85	16.972	−0.0733017	18.750	−0.0791631
37.95	17.003	−0.0735100	18.778	−0.0793542
39.05	17.036	−0.0737274	18.805	−0.0795464
40.15	17.063	−0.0739261	18.823	−0.0797062
41.25	17.105	−0.0741909	18.859	−0.0799444
42.35	17.156	−0.0745019	18.901	−0.0802151
43.45	17.201	−0.0747932	18.940	−0.0804762
44.55	17.252	−0.0751160	18.983	−0.0807632
45.65	17.308	−0.0754690	19.031	−0.0810812
46.75	17.375	−0.0758780	19.088	−0.0814447
47.85	17.439	−0.0762869	19.142	−0.0818039
48.95	17.501	−0.0766990	19.195	−0.0821763

[a]The angle θ is in degrees, a is dimensionless, and b is in K^{-1}.

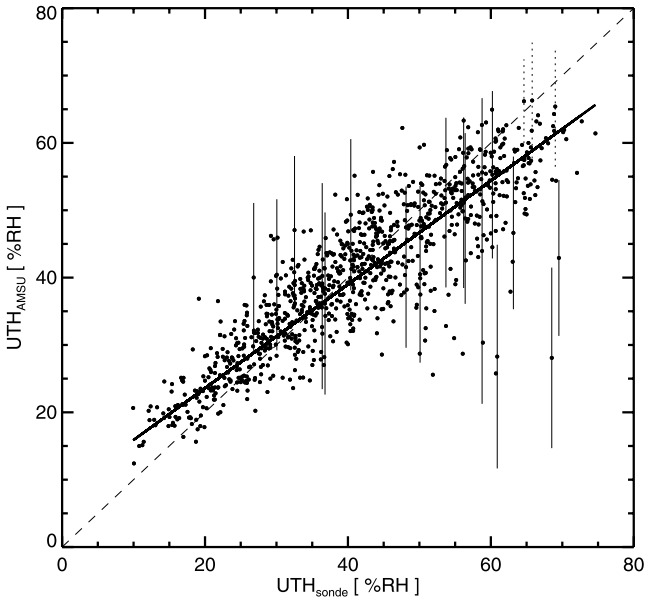

Figure 11. UTH_{AMSU} measured by AMSU versus UTH_{sonde} measured by radiosonde. Some example error bars are also shown only for highly inhomogeneous (solid vertical lines) and homogeneous (dotted vertical lines) cases to avoid clutter. The dashed line is the diagonal, and the solid line is the result of a least squares fit taking into account the varying error bars.

comparison. The most important reason for additional noise in the validation is atmospheric inhomogeneity on the 10 km scale. One can estimate this from σ_{50km}, the standard deviation of the AMSU radiances within a target area of 50 km radius, as discussed in BKJ. The total noise present in the intercomparison between simulated Lindenberg radiosonde radiances and measured AMSU radiances was found in BKJ to have a standard deviation of approximately 1.6 K. Putting this instead of the pure radiometric noise into the error estimate from the regression leads to absolute and relative UTH standard deviations of 8% RH and 19%, respectively, in close agreement with the standard deviations observed in the validation.

[39] Inspection of Figure 11 reveals that the points scatter not perfectly around the diagonal. Rather, UTH_{AMSU} seems to be higher than UTH_{sonde} at low UTH and lower than UTH_{sonde} at high UTH. To quantify this, one can fit a straight line to the data. However, the fit should take into account the varying error bars for each colocation. We use as error model

$$\sigma_{\Delta UTH}(\text{inhom}) = |b|\text{UTH}(0.5\,\text{K} + \sigma_{50km}), \qquad (12)$$

in analogy to (8), just replacing the radiometric noise by the error model derived in BKJ. This error is a measure for the uncertainty in the colocation. It is important to take it into account because it has a large variability. Figure 11 shows some sample error bars of $\sigma_{\Delta UTH}$(inhom). Note that this is not an error of the AMSU UTH itself, but a consequence of our inability to do a perfect colocation. The fit result is also shown in Figure 11. The parameters obtained are

$$UTH_{AMSU} = 8.2\%\text{RH} + 0.77UTH_{sonde}. \qquad (13)$$

The nonunity slope can be explained by a combination of three factors. Factor one is that the radiosondes seem to underestimate the UTH for very dry conditions, as shown in BKJ. Factors two and three are that the BT transformation method overestimates UTH for dry conditions and underestimates UTH for very moist conditions, as shown by Figure 5. All three factors act to decrease the slope of the fitted line. Taking this into account one can say that the agreement is quite reasonable. Particularly, there is no evidence for an overestimation of UTH for moist conditions due to cloud contamination.

[40] The reasonable agreement between Lindenberg radiosondes and AMSU UTH gives some confidence that the BT transformation method works well for microwave data. It would be desirable to do this kind of comparison also for other radiosonde stations, in particular for stations in other climate zones. Such comparisons are planned. However, they can be regarded as an investigation of the quality of the radiosonde data, rather than a validation of the BT transformation method, due to the rather poor quality of the global radiosonde data record.

3.3. Supersaturation

[41] Regions in the upper troposphere where the humidity concentration is supersaturated with respect to ice have received some attention recently [*Gierens et al.*, 1999; *Spichtinger et al.*, 2002; *Buehler and Courcoux*, 2003]. Can the BT transformation method be used to study the frequency of occurrence of supersaturation? Figure 12 shows histograms of UTH values, in this case with respect to ice, for the ECMWF data set. We denote the reference to

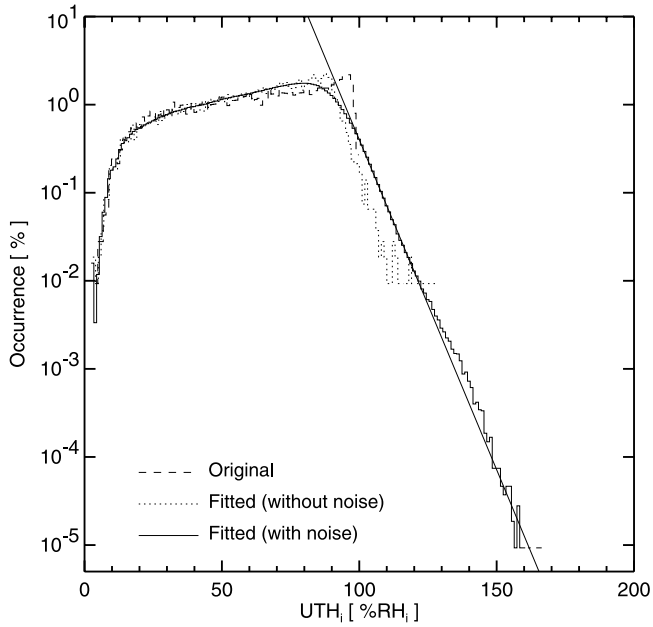

Figure 12. Histograms of UTH with respect to ice for the ECMWF data set. Shown are histograms for the true UTH_i (dashed line), for the retrieved UTH_i without radiometric noise (dotted line), and for the retrieved UTH_i with 1 K radiometric noise (solid line). The diagonal solid line shows an exponential fit to the supersaturated region of the histogram with noise (100 to 130% RH_i). The bin size for the histograms is 1% RH_i.

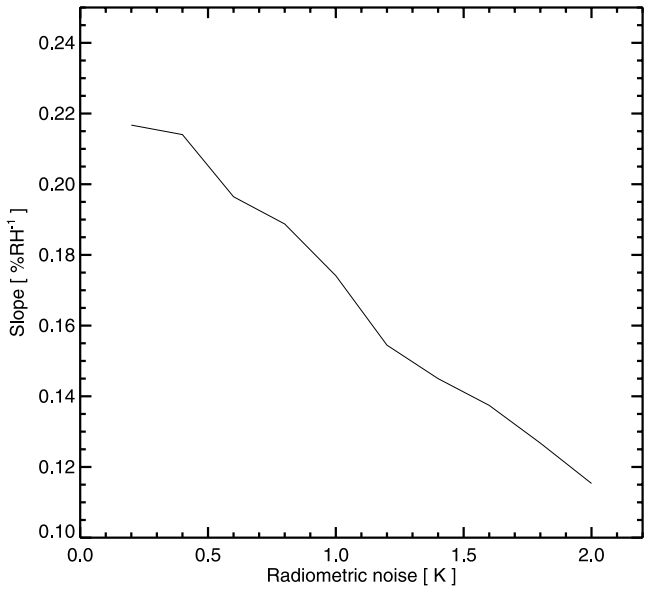

Figure 13. The value of the apparent supersaturation drop-off slope B as a function of the assumed radiometric noise standard deviation.

ice instead of liquid water with a subscript '$_i$'. UTH_i values above 100% RH_i are supersaturated. The 'true' UTH_i does not show any supersaturation. This is no surprise, since all profiles were taken from ECMWF analyses, which do not have any supersaturation due to the simple model cloud microphysics. That the ECMWF data does not show ice supersaturation can also be seen from the sharp cutoff in UTH_{true} at 70% RH in Figure 4 (right), since 70% RH corresponds approximately to 100% RH_i for typical upper tropospheric temperatures. (Figure 4 shows UTH_{true} values up to 90% RH for the TIGR-3 data set, so the TIGR-3 data set, which is based on radiosondes, does show ice supersaturation.)

[42] Interestingly, the retrieved UTH_i (dotted curve in Figure 12) does show ice supersaturation, due to the regression noise. The apparent ice supersaturation becomes even stronger when realistic radiometric noise of 1 K standard deviation is added (solid curve). For this last curve 1000 different random noise values were added for each ECMWF profile, so the histogram is based on a total of 10^7 UTH_{fitted} values. This Monte Carlo–type error analysis method is similar to the one described in detail by *Buehler and Courcoux* [2003]. Although the distribution of the radiometric noise is Gaussian, the supersaturation drop-off is exponential, due to the nonlinear mapping by relation (1). Following *Buehler and Courcoux* [2003] and the earlier study by *Spichtinger et al.* [2002], one can analyze the frequency of supersaturation quantitatively by fitting to the data an exponential of the form

$$p(\mathrm{UTH}_i) = Ae^{-B\ \mathrm{UTH}_i}, \tag{14}$$

where $p(UTH_i)$ is the frequency of occurrence of each supersaturated UTH_i value and A and B are fit coefficients. Such a fit is also displayed in Figure 12, the drop-off slope B is 0.17% RH^{-1} for this noise level.

[43] The value of B depends on the assumed radiometric noise level, as demonstrated by Figure 13, which was generated by repeating the analysis as displayed in Figure 12 for different radiometric noise standard deviations in steps of 0.2 K. The higher the radiometric noise, the slower the drop-off, the smaller B. Figure 13 can be used to define a detection threshold for true supersaturation: The drop-off slope B for the measured UTH_i must be significantly smaller than the one expected from the radiometric noise.

[44] The slope found by *Gierens et al.* [2004] from HIRS infrared data is 0.12, whereas the expected slope from an assumed worst case HIRS radiometric noise of 1 K is 0.17, so there would be indeed evidence for ice supersaturation. A devil's advocate would have to postulate a total noise level of 2 K to explain a supersaturation drop-off slope of 0.12 in the absence of real supersaturation. The above arguments assume that our analysis for microwave data is valid also for infrared data. This is of course not strictly true, because the transformation parameters a and b of relation (1) are different. However, the general behavior is expected to be the same. To get the exact numbers, a similar analysis could easily be carried out for infrared data as well.

4. Summary and Conclusions

[45] The properties of the BT transformation method applied to microwave data were investigated. The method can be used to retrieve Jacobian weighted upper tropospheric humidity (UTH) in a broad layer centered roughly between 6 and 8 km altitude. Retrieval results are sensitive to the type of Jacobian used to define UTH. It was found that the retrieval of UTH based on the fractional water vapor VMR Jacobian works better than the more traditional retrieval of UTH based on the relative humidity Jacobian, and that the new UTH definition does not need a reference pressure in the regression relation.

[46] The UTH bias is always below 4% RH, where the largest values are found for high-humidity cases. The UTH relative bias is always below 20%, where the largest values are found for low humidity cases. The UTH standard deviation is between 2 and 6.5% RH in absolute numbers, or between 10 and 27% in relative numbers. The standard deviation is dominated by the regression noise, resulting from vertical structure not accounted for by the simple transformation relation. The part of the UTH error resulting only from radiometric noise scales with the UTH value and has a relative standard deviation of approximately 7% for a radiometric noise level of 1 K. The UTH retrieval performance was shown to be of almost constant quality for all viewing angles and latitudes, except for problems at high latitudes due to surface effects.

[47] A comparison of AMSU UTH and radiosonde UTH for the radiosonde station Lindenberg was used to validate the retrieval method. The agreement is reasonable if known systematic differences between AMSU and radiosonde are taken into account.

[48] Additionally, it was investigated whether the method is suitable to study humidity supersaturation in the upper troposphere. In principle it is, but the regression noise and radiometric noise could lead to apparent supersaturation even if there were no supersaturation. For a radiometer noise level of 1 K the drop-off slope of the apparent

supersaturation is 0.17% RH^{-1}, for a noise level of 2 K the slope is 0.12% RH^{-1}.

[49] The main conclusion from this study is that the BT transformation method is very well suited for microwave data. Its particular strength is in climatological applications where the simplicity and the independence of a priori information are key advantages. Further studies applying the method to global and regional data are planned.

[50] **Acknowledgments.** Thanks to F. Chevallier and N. A. Scott for ECMWF and TIGR-3 data respectively, to Ulrich Leiterer and Horst Dier from DWD station Lindenberg for their radiosonde data, and to Lisa Neclos from the Comprehensive Large Array-data Stewardship System (CLASS) of the US National Oceanic and Atmospheric Administration (NOAA) for AMSU data. Thanks to K. Gierens and to two anonymous reviewers for their valuable and constructive comments on the manuscript. Last but not least, thanks to the ARTS radiative transfer community, many of whom have indirectly contributed by implementing features to the ARTS model. This study was funded by the German Federal Ministry of Education and Research (BMBF), within the AFO2000 project UTH-MOS, grant 07ATC04. It is a contribution to COST Action 723 'Data Exploitation and Modeling for the Upper Troposphere and Lower Stratosphere'.

References

Anderson, G. P., S. A. Clough, F. X. Kneizys, J. H. Chetwynd, and E. P. Shettle (1986), AFGL atmospheric constituent profiles (0–120 km), *Tech. Rep. TR-86-0110*, Air Force Geophys. Lab., Bedford, Mass.

Bates, J. J., and D. L. Jackson (2001), Trends in upper-tropospheric humidity, *Geophys. Res. Lett.*, *28*(9), 1695–1698.

Buehler, S. A., and N. Courcoux (2003), The impact of temperature errors on perceived humidity supersaturation, *Geophys. Res. Lett.*, *30*(14), 1759, doi:10.1029/2003GL017691.

Buehler, S. A., M. Kuvatov, V. O. John, U. Leiterer, and H. Dier (2004), Comparison of microwave satellite humidity data and radiosonde profiles: A case study, *J. Geophys. Res.*, *109*, D13103, doi:10.1029/2004JD004605.

Buehler, S. A., P. Eriksson, T. Kuhn, A. von Engeln, and C. Verdes (2005), ARTS, the atmospheric radiative transfer simulator, *J. Quant. Spectrosc. Radiat. Transfer*, *91*(1), 65–93, doi:10.1016/j.jqsrt.2004.05.051.

Burns, B. A., X. Wu, and G. R. Diak (1997), Effect of precipitation and cloud ice on brightness temperatures in AMSU moisture channels, *IEEE Trans. Geosci. Remote Sens.*, *35*(6), 1429–1437.

Chaboureau, J.-P., A. Chedin, and N. A. Scott (1998), Remote sensing of the vertical distribution of atmospheric water vapor from the TOVS observations: Method and validation, *J. Geophys. Res.*, *103*(D8), 8743–8752.

Chevallier, F. (2001), Sampled databases of 60-level atmospheric profiles from the ECMWF analysis, *EUMETSAT SAF Program Res. Rep 4*, Eur. Cent. for Medium-Range Weather Forecast., Reading, U. K.

Elliot, W. P., and D. J. Gaffen (1991), On the utility of radiosonde humidity archives for climate studies, *Bull. Am. Meteorol. Soc.*, *72*, 1507–1520.

Engelen, R. J., and G. L. Stephens (1998), Comparison between TOVS/HIRS and SSM/T-2 derived upper tropospheric humidity, *Bull. Am. Meteorol. Soc.*, *79*(12), 2748–2751.

Engelen, R. J., and G. L. Stephens (1999), Characterization of water-vapor retrievals from TOVS/HIRS and SSM/T-2 measuremets, *Q. J. R. Meteorol. Soc.*, *125*, 331–351.

Escoffier, C., J. J. Bates, A. Chedin, W. B. Rossow, and J. Schmetz (2001), Comparison of upper tropospheric humidity retrievels from TOVS and Meteosat, *J. Geophys. Res.*, *106*, 5227–5238.

Gierens, K., U. Schumann, M. Helten, H. Smit, and A. Marenco (1999), A distribution law for relative humidity in the upper troposphere and lower stratosphere derived from three years of MOZAIC measurements, *Ann. Geophys.*, *17*, 1218–1226.

Gierens, K., R. Kohlhepp, P. Spichtinger, and M. Schroedter-Homscheidt (2004), Ice supersaturation as seen from TOVS, *Atmos. Chem. Phys.*, *4*, 539–547.

Greenwald, T. J., and S. A. Christopher (2002), Effect of cold clouds on satellite measurements near 183 GHz, *J. Geophys. Res.*, *107*(D13), 4170, doi:10.1029/2000JD000258.

Harries, J. E. (1997), Atmospheric radiation and atmospheric humidity, *Q. J. R. Meteorol. Soc.*, *123*, 2173–2186.

Held, I. M., and B. J. Soden (2000), Water vapor feedback and global warming, *Annu. Rev. Energy Environ.*, *25*, 441–475.

Jackson, D. L., and J. J. Bates (2001), Upper tropospheric humidity algorithm assessment, *J. Geophys. Res.*, *106*(D23), 32,259–32,270.

Leiterer, U., H. Dier, and T. Naebert (1997), Improvements in radiosonde humidity profiles using RS80/RS90 radiosondes of Vaisala, *Contrib. Atmos. Phys.*, *70*(4), 319–336.

Melsheimer, C., et al. (2004), Intercomparison of general purpose clear sky atmospheric radiative transfer models for the millimeter/submillimeter spectral range, *Radio Sci*, doi:10.1029/2004RS003110, in press.

Rosenkranz, P. W. (2001), Retrieval of temperature and moisture profiles from AMSU-A and AMSU-B measurements, *IEEE Trans. Geosci. Remote Sens.*, *39*(11), 2429–2435.

Saunders, R. W., T. J. Hewison, S. J. Stringer, and N. C. Atkinson (1995), The radiometric characterization of AMSU-B, *IEEE Trans. Microwave Theory*, *43*(4), 760–771.

Soden, B. J., and F. P. Bretherton (1993), Upper tropospheric relative humidity from the GOES 6.7 μm channel: Method and climatology for July 1987, *J. Geophys. Res.*, *98*, 16,669–16,688.

Soden, B. J., and F. P. Bretherton (1996), Interpretation of TOVS water vapor radiances in terms of layer-average relative humidities: Method and climatology for the upper, middle, and lower troposphere, *J. Geophys. Res.*, *101*, 9333–9343.

Soden, B. J., D. D. Turner, B. M. Lesht, and L. M. Miloshevich (2004), An analysis of satellite, radiosonde, and lidar observations of upper tropospheric water vapor from the Atmospheric Radiation Measurement Program, *J. Geophys. Res.*, *109*, D04105, doi:10.1029/2003JD003828.

Sohn, B. J., E.-S. Chung, J. Schmetz, and E. A. Smith (2001), Estimating upper-tropospheric water vapor from SSM/T-2 satellite measurements, *J. Appl. Meteorol.*, *42*, 488–504.

Spencer, R. W., and W. D. Braswell (1997), How dry is the tropical free troposphere? Implications for global warming theory, *Bull. Am. Meteorol. Soc.*, *78*(6), 1097–1106.

Spichtinger, P., K. Gierens, and W. Read (2002), The statistical distribution law of relative humidity in the global tropopause region, *Meteorol. Z.*, *11*, 83–88.

Tian, B., B. J. Soden, and X. Wu (2004), Diurnal cycle of convection, clouds, and water vapor in the tropical upper troposphere: Satellite versus a general circulation model, *J. Geophys. Res.*, *109*, D10101, doi:10.1029/2003JD004117.

Wilheit, T. T. (1990), An algorith for retrieving water vapor profiles in clear and cloudy atmospheres from 183-GHz radiometric measurements: Simulation studies, *J. Appl. Meteorol.*, *29*, 508–515.

S. A. Buehler and V. O. John, Institute of Environmental Physics, University of Bremen, Otto-Hahn-Allee 1, D-28359 Bremen, Germany. (sbuehler@uni-bremen.de)